American Mineralogist, Volume 79, pages 340–352, 1994

Sector-zoned aegirine from the Ilímaussaq alkaline intrusion, South Greenland: Implications for trace-element behavior in pyroxene

C. K. Shearer
Institute of Meteoritics, Department of Earth and Planetary Sciences, University of New Mexico, Albuquerque, New Mexico 87131-1126, U.S.A.

L. M. Larsen
The Geological Survey of Greenland, Øster-Voldgade 10, DK-1350 Copenhagen K, Denmark

Abstract

Sector-zoned aegirine crystals from a peralkaline nepheline syenite in Ilímaussaq, South Greenland, have been analyzed for major and trace elements using combined electron microprobe and secondary-ion mass spectrometry techniques. Unlike in calcic clinopyroxene, the faster growing basal sector of the sodic clinopyroxene is enriched in incompatible elements such as Sr, REE, and Zr relative to the slower growing prism sectors. The prism sectors are enriched in Al and Ti relative to the basal sector, but the Al-Ti enrichment patterns in the prism sectors contrast with those in calcic clinopyroxene. Zr, REE, and Sr exhibit a positive correlation to Ca in the M2 site and a negative correlation to Na in the M2 site.

The contrasts we report between aegirine and augite demonstrate that site characteristics and the ability of a site to accommodate a cation are important factors for controlling sector enrichments. The addition of an acmite component [Ca (M2) + Fe^{2+} (M1) ↔ Na (M2) + Fe^{3+} (M1)] to the pyroxene results in a shift of the optimum potential radius for cations accommodated in the M1 and a change in the ideal charge characteristic of the M2 site. Those cations with radii that deviate the farthest from the optimum M1 and M2 site radii and ideal charge for a particular pyroxene composition have a greater probability of being retained in a faster growing basal sector than in the more slowly growing prism sector. These observations do not, however, eliminate a model in which adsorption and desorption kinetics plays an important role in the differences among sectors in major components [i.e., Na/(Na + Ca) and $Fe^{3+}/(Fe^{2+} + Fe^{3+})$]. This mechanism may then ultimately be responsible for the differences in crystal chemistry or geometric factor among sector growth surfaces.

Introduction

Chemical sector zoning occurs when different growth sectors or face loci of a single crystal have significantly different compositions (Hollister, 1970; Hollister and Gancarz, 1971; Dowty, 1976). These compositional differences are produced on surfaces of simultaneously growing crystal faces under identical conditions (Hollister and Gancarz, 1971). The existence of sector zoning clearly indicates disequilibrium crystallization (Leung, 1974; Shimizu, 1981; Paquette and Reeder, 1990a, 1990b). Sector zoning, therefore, provides a perspective into diffusional and interface kinetic mechanisms controlling trace-element behavior under disequilibrium conditions (Albarede and Bottinga, 1972; Shimizu, 1981).

Chemical sector zoning has been described in numerous synthetic compounds and naturally occurring minerals (see Dowty, 1976, and Leung, 1974, for summary). Perhaps the best documented sector zoning in silicates is in pyroxene (Strong, 1969; Hollister and Gancarz, 1971; Bence and Papike, 1971, 1972; Thompson, 1972; Ferguson, 1973; Nakamura, 1973; Nakamura and Coombs, 1973; Leung, 1974; Downes, 1974; Dowty, 1976, 1977; Harkins and Hollister, 1977; Carpenter, 1980; Shimizu, 1981; Larsen, 1981; Kouchi et al., 1983). Several models have been designed to explain chemical sector zoning in pyroxene. The model proposed by Hollister (1970) and Hollister and Gancarz (1971) is based on the concept that local charge balance is maintained by charge-compensatory cation substitutions into completed sites on the growth surfaces. Differences in the atomic configuration on growth surfaces and the nature of the prominent substitutions are important variables. Nakamura (1973), Dowty (1976, 1977), and Shimizu (1981) suggested that the adsorption and desorption of cations into partially completed sites on the growth surfaces is an important mechanism for the development of sector zoning. Growth surfaces with favorable protosite configurations are thereby preferentially enriched. Adsorption of elements into protosites is proportional to the charge to size ratio of the cation. Therefore, in contrast to the model of Hollister (1970) and Hollister and Gancarz (1971), coupled cation substitutions do not necessarily have to compensate for

0003–004X/94/0304–0340$02.00

charge balancing within a single growth step or layer, and partition coefficients for all elements approach one. Kouchi et al. (1983) concluded that sector enrichment was related to the effect of supercooling on the crystal growth mechanism (i.e., spiral growth, two-dimensional nucleation growth, layer growth, and crystallographic orientation of growth steps) and to surface kinetics. Changing crystal growth mechanisms should result in a changing site (or protosite) configuration of the growth surfaces. The importance of such mechanisms has been documented in carbonates (Paquette and Reeder, 1990a, 1990b; Reeder, 1992). Compositional differences among growth sectors has also been attributed to the interplay between growth rates of growth surfaces and the relative diffusion rates of cationic species in the melt (Downes, 1974; Larsen, 1981).

Previous studies of minor- and trace-element incorporation into growth sectors of pyroxene have focused upon clinopyroxene in which the M2 site is primarily occupied by Ca^{2+} (Shimizu, 1981; Kouchi et al., 1983). This study focuses upon sector-zoned pyroxene with substantial Na^{+} in the M2 site. This difference in M2 occupancy influences the character of sector enrichments and provides additional insight into the mechanisms involved in crystal growth, the formation of chemical sector zoning, and trace-element substitution.

Occurrence of sector-zoned aegirine

Sector zoning in aegirine has been described from alkaline plutonic and hydrothermal rocks (Larsen, 1976, 1981; Ranløv and Dymek, 1991). The feature may be more common in such rocks than generally realized because it may be difficult to identify. The material used in this investigation comes from the Ilímaussaq alkaline intrusion in South Greenland, from one of the samples (GGU 91969) that was also used by Larsen (1981). The Ilímaussaq intrusion consists of an early intrusion of augite syenite followed by a layered complex of peralkaline (agpaitic) nepheline syenites: sodalite foyaite, naujaite, kakortokite, and lujavrite (Ussing, 1912; Ferguson, 1964, 1970; Larsen, 1976). Sector zoning is frequently observed in aegirine from the sodalite foyaite and naujaite. Sector zoning is less common or absent in the other rock types (Larsen, 1981). Aegirine from the sodalite foyaite was selected for this study. The mineral assemblage in the sodalite foyaite consists of alkali feldspar, sodalite, nepheline, hedenbergite, fayalite, titanomagnetite, katophorite, eudialyte, aenigmatite, aegirine, arfvedsonite, analcime, and rinkite (Larsen, 1981). The crystallization sequence among these minerals has been summarized by Larsen (1976, 1977).

The aegirine in the sodalite foyaite forms subhedral to euhedral prismatic crystals 0.1–10 mm long. The crystals are elongated in the **c** direction and are somewhat platy parallel to {100}. The dominating forms are {100} and {110}. The form under which the basal sector grew has not been identified with certainty. This sector has been denoted by Larsen (1981) by the zone symbol [001], a designation proposed by Harkins and Hollister (1977). Boundaries between sectors are usually not straight but possess curvatures indicative of differences in the relative growth rates of the sectors. The relative growth rates of the various sectors as deduced from morphology by Larsen (1981) are [001] > {010} > {110} > {100}.

Analytical techniques

After optical observation and preliminary microbeam analysis of several aegirine grains from the sodalite foyaite, a single sector-zoned aegirine crystal from sample GGU 91969 was analyzed in detail with electron microprobe (EMP) analysis and secondary ion mass spectrometry (SIMS). Sectors within the crystal were distinguished based on the criteria of Larsen (1981) for similar aegirine crystals in the Ilímaussaq intrusion. A photograph of the sector-zoned aegirine crystal, a reconstruction of the sector zoning, and EMP-SIMS points are shown in Figure 1.

Prior to SIMS and electron microprobe analysis, the crystal was photographed to document analysis locations precisely. In addition, backscattered electron imaging and preliminary microprobe analyses documented both sector and concentric zoning. To provide combined SIMS and EMP analyses of identical points, it was decided to perform SIMS analyses prior to detailed EMP analysis. SIMS analysis craters are relatively easy to locate for subsequent EMP analysis.

The SIMS analyses were obtained with a Cameca IMS 3f ion probe located at the Woods Hole Oceanographic Institute. Rare earth element analyses were carried out with a primary O^{-} ion beam, which was 25–30 μm in diameter. Moderate energy filtering was used to remove molecular ion interferences (Shimizu and Hart, 1981). The data for a second set of trace elements (Zr, Ti, Cr, V, Sr, Y) were obtained with a primary O^{-} ion beam 5–8 μm in diameter and with more stringent energy filtering (90 V offset). The secondary ion intensities were measured by an electron multiplier coupled with pulse-counting circuitry. All concentrations were calculated from empirical relationships between intensity ratios relative to Si (as Ce/Si) and concentrations (i.e., working curves) obtained from well-documented standards (Irving and Frey, 1984; Shimizu, unpublished data). Accuracy and precision for REE data are 15% or less and <10% for Y, Ti, V, Zr, and Sr.

Following SIMS analysis, the points adjacent to SIMS spots were analyzed for major and minor elements using a JEOL 733 electron microprobe equipped with an Oxford-Link system at the University of New Mexico. Mineral analyses were obtained using mineral and oxide standards, an acceleration voltage of 15 KeV, and a beam diameter of 2–5 μm. Measured X-ray intensities were reduced according to the method of Bence and Albee (1968).

Crystal chemistry of pyroxene

The pyroxene group minerals crystallize in a variety of space groups, but for our purposes only the *C*2/*c* for au-

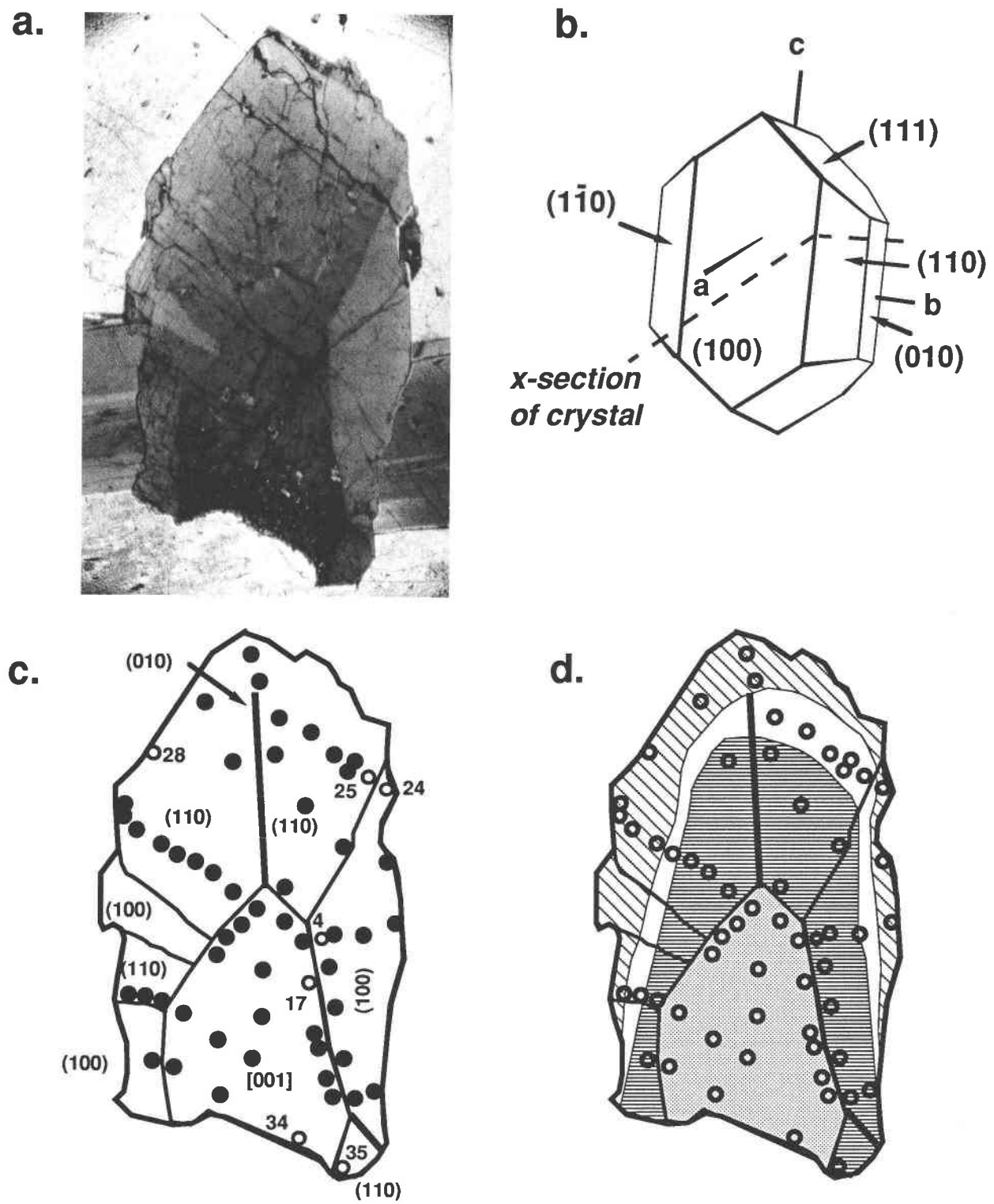

Fig. 1. (**a**) Photograph of one of the aegirine crystals used in this study. The aegirine is approximately 6 mm in length. (**b**) Idealized section (dashed line), which approximates the orientation of **a**. (**c**) Identified sectors and EMP-SIMS analyses points. Location of analyses in Table 1 are designated by number and open point. (**d**) Na/(Na + Ca) zoning in crystal. Patterns representing Na/(Na + Ca) values are as follows: dotted = <0.80, horizontal lines = 0.85–0.90, white = 0.90–0.95, and inclined lines = 0.95–0.98.

gite and aegirine are important. The pyroxene structure can be described in terms of alternating tetrahedral and octahedral layers that lie parallel to the (100) plane. The tetrahedral layer is composed of infinite chains of corner-sharing tetrahedra running parallel to **c**. The octahedral layer is composed of the sixfold- to eightfold-coordinated sites. M1 octahedra share edges to form infinite chains parallel to **c**. The M2 polyhedra are either sixfold or eightfold coordinated, depending on their occupancy. The site is eightfold coordinated when it contains Ca or Na but is approximately sixfold coordinated when containing smaller cations. Shearer et al. (1989) and McKay (1989) reviewed the impact of M1 and M2 site characteristics on trace-element behavior.

Parameters describing M1 and M2 site characteristics for diopside, hedenbergite, and acmite can be calculated based on the methods used by Smyth and Bish (1988), Caporuscio and Smyth (1990), and Smyth (1992). Using the data of Smyth and Bish (1988), we calculated the cation site radii, site electrostatic potential, and optimal cation charge for M1 and M2 sites in hedenbergite and acmite (Table 1). The data in Table 1 for diopside were calculated by Caporuscio and Smyth (1990). Over the compositional range from hedenbergite to acmite, the M2 site radius varies by <1%. The optimal cation charge varies by approximately 54%. The M1 site over the same compositional range shows a different relationship. The M1 site radius varies by 5%, whereas the optimal charge varies by 23%.

As demonstrated by Dowty (1976), the growth sectors {100}, {110}, {010}, and {$\bar{1}$11} have different surface site configurations. Surfaces of least bonding parallel to {$\bar{1}$11} expose only M2 sites or M1 sites with four of the six octahedral bonds directed toward the crystal (4/6 site using the terminology of Nakamura, 1973) (Dowty, 1976). Both the {110} and {010} surfaces expose M1 sites, with four of the six octahedral bonds and four of the eight cubic bonds directed toward the crystal. The {100} surface has both M1 and M2 sites simultaneously exposed, with three of the six octahedral bonds and four of the eight cubic bonds directed toward the crystal. The (100) surface has four times the number of M1 and M2 sites with advantageous configurations (Dowty, 1976) than the {$\bar{1}$11} surface. Hollister (1970), Hollister and Gancarz (1971), Kouchi et al. (1983), Paquette and Reeder (1990a, 1990b), and Reeder (1992) noted that the surface configuration perpendicular to the growth direction was not the only important structural variable in cation substitution. They suggested that different growth mechanisms may be important in exposing different site configurations. For example, in pyroxene the dislocation step to {100} has both tetrahedral and M1 sites simultaneously exposed on the growth surface, whereas M1 and M2 are simultaneously exposed on the {100} surface (Hollister, 1970; Hollister and Gancarz, 1971). Kouchi et al. (1983) illustrated that the style of the growth mechanism may be influenced by the degree of supercooling.

Table 1. Characteristics of M1 and M2 sites in clinopyroxene

	Diopside*	Hedenbergite*	Acmite**
	M1 site		
Radius (pm)	67.7	73.1	62.5
Site energy (kcal/mol)	−1284	−1232	−2424
Potential (V)	−27.86	−26.7	−35.03
Ideal charge	2.40	2.30	3.02
	M2 site		
Radius (pm)	109.8	111.1	111.9
Site energy (kcal/mol)	−957	−960	−308
Potential (V)	−20.75	−20.80	−13.4
Ideal charge	1.79	1.79	1.16

* Cameron et al. (1973), Smyth and Bish (1988).
** Clark et al. (1969), Smyth and Bish (1988).

Analytical results

Major- and minor-element microprobe analyses of the pyroxene grain analyzed are summarized in Table 2. Cation formulas including Fe^{2+} and Fe^{3+} were calculated assuming four cations and six O atoms in the formula (e.g., Robinson, 1980). The pyroxene analyzed for this study has limited pyroxene quadrilateral components. The only quadrilateral component observed is $CaFe^{2+}Si_2O_6$, which ranges from 2 to 26%. Larsen (1981) observed that this component reached 0% in other sector-zoned aegirine crystals from the same intrusion where no Fe^{2+} remained after recalculation. The nonquadrilateral components involve Na substitution in the M2 site and Al, Ti, and Fe^{3+} substitution in the M1 site. The dominant other components in these pyroxenes are acmite and jadeite. The acmite component ranges from approximately 75 to 90% and reflects the coupled substitution Ca^{2+} (M2) + Fe^{2+} (M1) ↔ Na^{1+} (M2) + Fe^{3+} (M1). The jadeite component ranges from 2 to 10% and reflects the coupled substitution Ca^{2+} (M2) + Fe^{2+} (M1) ↔ Na^{1+} (M2) + Al^{3+} (M1). Ti^{4+} (<2%) is most likely incorporated by the following coupled substitutions: $(Fe,Al)^{3+}$ (M1) ↔ $0.5Fe^{2+}$ (M1) + 0.5 $(Zr,Ti)^{4+}$ (M1) (Larsen, 1981; Ranløv and Dymek, 1991) and Ca^{2+} (M2) + 0.5 Fe^{2+} (M1) ↔ Na^{1+} (M2) + $0.5Ti^{4+}$ (M1). Other potential coupled substitutions involving Ti and Al are unlikely because aegirine has a very low content of $^{[4]}Al$ (Deer et al., 1978; Nielsen, 1979; Larsen, 1981; Czamanske and Atkin, 1985; Ranløv and Dymek, 1991).

Major-element concentric zoning in individual sectors is dominated by the variability in acmite and hedenbergite components. The sector and concentric zoning illustrated in Figure 1d depicts Na/(Na + Ca) variation in the aegirine crystal. Within the individual sectors the sodic components increase from core [Na/(Na + Ca) = 0.78] to rim [Na/(Na + Ca) = 0.97].

As observed by Larsen (1981), the individual sectors show specific individual enrichment schemes (Table 3). The hedenbergite component ($CaFe^{2+}Si_2O_6$) is enriched in the basal sector [001] relative to the prism sectors. Larsen (1981) concluded that the order of Ca enrichment in the prism sectors is {110} > {100} > {010}. Obvi-

TABLE 2. Selected analyses of pyroxene grain in Fig. 1

Analysis	{100}		[001]		{110}		
no.	4	24	17	34	25	28	35
SiO_2	50.45	51.62	50.08	51.07	51.61	52.00	51.03
TiO_2	0.63	0.79	0.37	0.42	1.30	0.52	1.16
ZrO_2	0.52	0.15	1.18	1.13	0.40	0.17	0.41
Al_2O_3	0.96	1.07	0.66	0.75	1.04	1.72	1.22
Fe_2O_3	28.07	31.41	24.90	25.00	27.93	30.13	26.42
FeO	3.38	0.19	5.21	6.24	2.98	0.81	3.74
MnO	0.19	0.22	0.33	0.38	0.24	0.40	0.24
MgO	0.02	0.00	0.02	0.04	0.00	0.01	0.00
CaO	3.44	1.00	5.70	5.28	2.26	1.13	3.56
Na_2O	11.41	13.03	10.09	10.64	12.29	12.97	11.57
Total	99.07	99.29	98.54	100.95	100.05	99.86	99.35
Formula based on four cations and six O atoms							
Si	1.980	1.992	2.002	2.006	1.991	1.993	1.986
Al	0.020	0.008	0.000	0.000	0.009	0.007	0.014
T_{tot}	2.000	2.000	2.002	2.006	2.000	2.000	2.000
Al	0.024	0.034	0.021	0.035	0.039	0.071	0.042
Ti	0.018	0.023	0.011	0.013	0.038	0.015	0.034
Fe^{3+}	0.828	0.906	0.748	0.721	0.810	0.868	0.774
Fe^{2+}	0.111	0.013	0.174	0.200	0.096	0.026	0.122
Mn	0.007	0.007	0.013	0.012	0.008	0.011	0.008
Mg	0.000	0.000	0.000	0.003	0.000	0.000	0.000
$M1_{tot}$	0.988	0.983	0.978	0.984	0.988	0.991	0.980
Ca	0.144	0.041	0.245	0.220	0.092	0.046	0.148
Na	0.868	0.974	0.777	0.815	0.917	0.963	0.872
$M2_{tot}$	1.012	1.015	1.022	1.035	1.009	1.009	1.020
Trace elements (SIMS) (ppm)							
Ce	35.8	5.7	37.4	81.3	15.4	8.0	35.5
Nd	13.2	1.4	15.3	24.0	4.2	1.9	16.7
Sm	2.9	0.3	3.7	9.3	0.9	0.4	3.2
Eu	0.2	0.02	0.3	1.0	0.08	0.02	0.2
Dy	1.2	0.2	2.0	8.2	0.5	0.5	1.5
Er	1.1	0.7	2.3	6.1	0.9	2.3	1.8
Yb	5.8	8.1	11.1	12.3	6.6	12.6	9.7
Ti	4120	6422	2500	2906	10056	3804	8000
V	6.5	9.1	5.9	6.3	7.2	7.2	8.4
Cr	1.5	2	1.6	1.5	1.5	1.7	2.4
Sr	4.0	3.3	4.8	7	5.1	3.2	4.2
Y	8.5	5.5	19.2	28.1	8.2	25.8	11.2
Zr	3825	1131	8763	8332	2922	1288	3061

Note: ZrO_2 = Zr from the ion probe and is not included in calculation of formula. Fe_2O_3 and FeO are calculated from Fe_{tot} and pyroxene stoichiometry. Points are located in Fig. 1c.

ously, the enrichment in the sodic components is the reverse. Larsen (1981) observed that the sector enrichment schemes for Na and Fe^{3+} were slightly different, with Na having {010} ≥ {100} > {110} > [001] and Fe^{3+} having {100} > {110} ≳ {010} > [001]. This difference is attributed to the jadeite component enrichment in the {010} sector.

Selected trace-element data for the pyroxene are presented in Table 2. The pyroxene shows high but variable abundances of LREE (Ce 5.7–82.8 ppm), HREE (4.5–26.1 ppm), Y (4.1–89.9 ppm), Zr (700–10680 ppm), and Ti (2898–11893 ppm). Trace elements such as Sr (2.5–8.3 ppm), Cr (1.4–2.4 ppm), and V (4.2–11.6 ppm) are lower in abundance and show much less variability. On the basis of our previous analysis of pyroxene site accommodation for trace elements, it is anticipated that the REE, Y, and Sr would be accommodated in the M2 site of pyroxene, whereas Al, Zr, V, Cr, and Ti would be better accommodated in the M1 site. (Shearer et al., 1989). To understand better the relationships between relative trace-element enrichments of individual sectors and major-element components, we calculated correlation coefficients among trace and major elements (Table 4).

The chondrite normalized patterns for the REE are enriched in both LREE (Ce) and HREE (Yb) and depleted in MREE (Sm, Eu, Dy) (Fig. 2). All have negative Eu anomalies. This pattern is unusual compared with quadrilateral pyroxenes (Shearer et al., 1989, 1991; McKay, 1989). Although we anticipated that MREE-oxide interferences would result in minor false enrichments in the HREE pattern, the ∪-shaped REE pattern appears to be real. This pattern is typical of Na- and Fe-enriched pyroxenes that crystallized from a peralkaline magma (Larsen, 1979; Mahood and Stimac, 1990) (Fig. 2a). We interpreted the ∪-shaped pattern of the aegirine as representing the interplay of pyroxene partition coefficients ($K_d^{HREE} > K_d^{LREE}$) and the LREE-enriched character with a negative Eu anomaly of the Ilímaussaq peralkaline magma. A typical whole rock pattern for these rock types is illustrated in Figure 2d.

TABLE 3. Sector enrichments and relative growth rates for the Ilímaussaq aegirine and augite

Element	Relative enrichment in aegirine	Relative enrichment in augite
Al	{010} ≫ {110} > {100} > [001]	{100} > {010} ≥ {110} > {$\bar{1}$11}*
Ti	{110} > {010} > {100} ≥ [001]	{100} > {010} ≥ {110} > {$\bar{1}$11}*
Fe^{3+}	{100} > {110} ≳ {010} > [001]	
Fe^{2+}	[001] > {110} > {010} ≳ {100}	
Fe_{tot}	[001] = {100} > {110} > {010}	{100} > {$\bar{1}$11}**
Mn	[001] ≥ {110} ≥ {100} = {010}	{100} ≈ {$\bar{1}$11}**
Ca	[001] > {110} > {100} > {010}	{100} > {$\bar{1}$11}**
Na	{010} ≥ {100} > {110} > [001]	{100} > {$\bar{1}$11}**
LREE	[001] ≫ {100} > {110}	{100} > {$\bar{1}$11}†
HREE	[001] > {100} > {110}	{100} > {$\bar{1}$11}†
Zr	[001] ≫ {100} ≥ {110}	{100} > {$\bar{1}$11}**
Y	[001] ≫ {100} ≥ {110}	{100} > {$\bar{1}$11}†
V	[001] = {110} = {100}	{100} > {$\bar{1}$11}**
Cr	[001] = {110} = {100} = {010}	{100} > {$\bar{1}$11}**
Sr	[001] > {110} = {100}	{100} > {$\bar{1}$11}**
Growth rate	relative growth rate in aegirine	relative growth rate in augite
	[001] > {010} > {110} > {100}	{$\bar{1}$11} > {100}**
		{$\bar{1}$11} > {100}, {110}, {010}‡

* Hollister and Gancarz (1971).
** Shimizu (1981).
† Predicted based on the observations made by Shimizu (1981).
‡ Leung (1974).

LREE and MREE are highly correlated with the cation substitutions in the M2 site (Table 4). Ce, Nd, Sm, Eu, and Dy have a high positive correlation with Ca and a high negative correlation with Na and Na/(Na + Ca). That is, an increase in the sodic components is correlated with a decrease in REE. The HREE such as Er and Yb appear not to be strongly correlated with major-element components in the M2 site. In addition, the REE are substantially enriched in the basal sector relative to the prism sectors (Tables 2 and 3 and Figs. 2 and 3). This contrasts with the observations of Shimizu (1981) for sector-zoned augite (Table 3). In the prism sectors of the aegirine, the REE are slightly more enriched in {100} relative to {110}.

Based on observations made on calcium clinopyroxene from basalts and eclogites, the REE concentration in clinopyroxene is dependent upon the nature of the REE substitution mechanism, the characteristics of the M2 site (i.e., optimal cation size and charge for the site), the concentration of REE in the magma, and the relative enrichment schemes in sector-zoned pyroxenes (McKay, 1989; Shearer et al., 1989; Caporuscio and Smyth, 1990). The relative importance of each of these variables in the observed correlation between REE and major M2 site components can be evaluated. Assuming charge balance, REE may be substituted into the M2 site of pyroxene through two possible coupled substitutions: 2Ca (M2) ↔ Na (M2) + REE (M2) and Ca (M2) + Si (T) ↔ REE (M2) + Al (T). If this mechanism solely controlled REE behavior, Ca and REE would show a negative correlation. Unlike for quadrilateral pyroxenes, in which Ca substitution into the M2 site props open the site and thereby increases the ability for REE to substitute into that site (Shearer et al., 1989; McKay, 1989), it is anticipated that substitutions of the type Na ↔ Ca will have a limited effect on the size of the M2 site. The similarity of mean M2 site size for hedenbergite (Cameron et al., 1973) and acmite (Clark et al., 1969) illustrate this point (Table 1). Therefore, this minor change in the size of the M2 site has a limited effect on the site's ability to accommodate cations such as the REE and does not account for the observed REE-Na-Ca correlations. Similar correlations among REE, Na, and Ca were observed by Caporuscio and Smyth (1990) in mantle eclogite pyroxenes along the diopside-jadeite solid solution. They attributed this correlation to dramatic differences in optimal charge characteristics between the M2 sites in diopside and jadeite (approximately 22%). The differences in the calculated optimal charge for the M2 sites in hedenbergite (1.79) and acmite (1.16) is therefore a dominant variable influencing the trace element substitution into the M2 site. Although the coupled substitution involving Na in M2 and smaller trivalent cations in M1 does not affect the size characteristics of the M2 site, it does affect the size characteristics of the M1 site (Cameron and Papike,1981; Table 1 of this paper). That has implications for trace-element substitutions into that site.

An additional variable that may be of importance is the magma composition. Crystallization of exotic REE-bearing phases (Larsen, 1977, 1979) would result in decreasing REE and Ca and increasing Na during pyroxene growth.

Zr^{4+} is most easily accommodated in the M1 site of clinopyroxene. The sector enrichment documented by Larsen (1981) and this study is [001] ≫ {100} > {010} > {110}. The sequence of sector enrichment for Zr is opposite to that of Ti. The enrichment of the basal sector compared with the prism sector contrasts with the observations made in augite (Shimizu, 1981). Zr shows a positive correlation to Ca in the M2 and a negative correla-

TABLE 4. Trace-element and major cation correlation coefficients for the aegirine

	Ti (M1)	Al (M1)	Ca (M2)	Na (M2)	Na/(Na + Ca)
Ce	−0.681	−0.469	0.880	−0.793	−0.892
Nd	−0.580	−0.438	0.779	−0.684	−0.786
Sm	−0.645	−0.507	0.835	−0.743	−0.845
Eu	−0.686	−0.537	0.877	−0.808	−0.895
Dy	−0.619	−0.508	0.835	−0.750	−0.850
Er	−0.121	−0.049	0.354	−0.220	−0.358
Yb	0.024	0.107	0.104	0.017	−0.103
Ti	1.000	0.791	0.424	0.466	0.437
V	0.158	0.071	−0.118	0.134	0.120
Cr	−0.238	−0.272	0.495	−0.416	−0.484
Sr	−0.486	−0.513	0.504	−0.469	−0.502
Y	−0.355	−0.236	0.496	−0.375	−0.486
Zr	−0.733	−0.677	0.752	−0.736	−0.767

tion to Na in the M2. Zr also shows a negative correlation with both Ti and Al, with which it competes for the M1 site. Again, with the assumption that charge balancing is required for Zr substitution into the M1 site, the possible substitutions are $0.5R^{2+}$ (M1) + Si (T) ↔ $0.5Zr^{4+}$ (M1) + Al (T) and 2Ca (M2) + R^{2+} (M1) ↔ 2Na (M2) + Zr^{4+} (M1). The former is less important because it requires substantial $^{[4]}$Al in the aegirine.

Sr, Cr, and V are all in very low concentrations in the aegirine. The basal sector shows a slight enrichment in Sr relative to the prism sectors (Table 3). This again contrasts with trace-element observations of Shimizu (1981). Cr and V appear not to be enriched in any particular sector, but that may be a function of their low concentrations and poorer analytical precision at these concentrations.

In summary, the sector enrichment for major-, minor-, and trace-elements for aegirine is different from that observed in other pyroxenes. In contrast to calcic pyroxenes, the study by Larsen (1981) and the present study (Table 3) indicate the following characteristics of sodic pyroxenes: (1) REE and Zr are enriched in the basal sector [001] rather than the prism sectors. (2) The REE and Zr sector enrichments generally appear to correspond with growth rate. The fastest growth sector is more enriched than the slowest growth sector. Sectors with intermediate growth rates tend to show more overlap. (3) REE and Zr decrease with increasing Na/(Na + Ca) from the interior of a sector to the perimeter of a sector. (4) As in other clinopyroxenes, Al and Ti are enriched in prism sectors relative to the basal sector. However, their sector enrichment among prism sectors in aegirine differs from that observed in other pyroxenes (Bence et al., 1970; Hollister and Gancarz, 1971; Thompson, 1972; Leung, 1974; Harkins and Hollister, 1977). Although several prism sector enrichment schemes in augite have been documented for Al and Ti, the {100} sector has always been observed to have higher contents of Al and Ti than the {010} sector. Larsen (1981) and this study indicate that the sector enrichment in aegirine for Al is {010} ≫ {110} > {100} > [001] and for Ti is {110} > {010} > {100} ≥ [001] (Table 3 and Fig. 3).

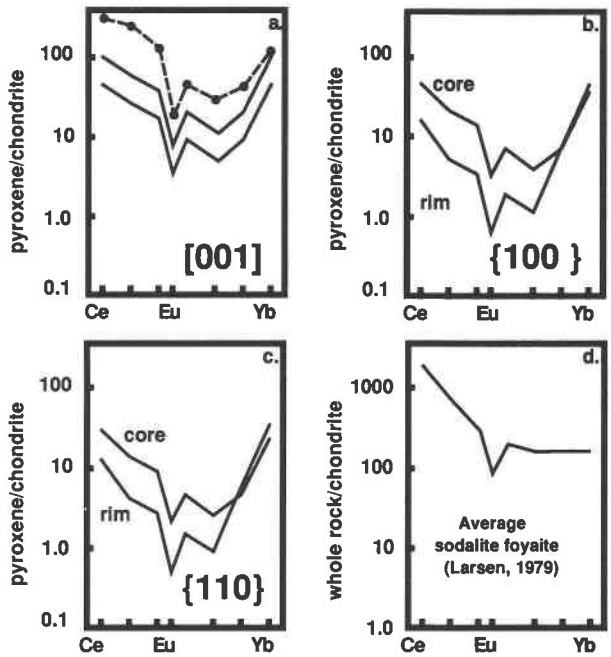

Fig. 2. Chondrite-normalized REE patterns for various sectors in the aegirine crystal shown in Fig. 1. (**a**) The [001] sector and a pattern of hedenbergite separate (dashed line) from foyaite (sample 91943: Larsen, 1979). (**b**) The {100} sector. (**c**) The {110} sector. (**d**) A whole-rock REE pattern for an undersaturated rock type from the Ilímaussaq alkaline intrusion (Larsen, 1979).

DISCUSSION

Role of diffusional vs. surface kinetic processes

When crystals grow in a magma, there are at least four processes that must be considered in a complete description of trace-element substitutions into structural sites. These are reactions occurring at the crystal-melt interface, the transport of species to that interface, the removal of latent heat generated during crystallization at the interface, and the bulk flow of magma. The relative importance and interplay among these processes may influence the relative enrichments observed in sector-zoned pyroxenes. For silicate materials, the interface processes and diffusion are usually considered the most important (Kirkpatrick, 1974, 1975, 1981). As pointed out by Kirkpatrick (1981), the removal of heat from the interface is of little significance because thermal diffusivities (10^{-2}–10^{-3} cm²/s) are several orders of magnitude larger than the diffusion coefficients (> 10^{-6} cm²/s). Although most calculations of composite gradients adjacent to crystal growth surfaces have assumed a static system, bulk flow may be important in natural magmatic systems. Shear, resulting from density or flow driven by surface tension, may disrupt compositional gradients established at a crystal-melt interface by diffusional processes (Anderson, 1984; Kirkpatrick, 1981). It has been treated sparingly in theoretical calculations (Shaw, 1974; Lasaga, 1981; Loomis, 1981; Anderson, 1984). In addition, bulk flow

may not be an important process in trace-element partitioning in these pyroxenes. The aegirine crystals considered here crystallized interstitially, within a framework of minerals in which the flow of melt would be very limited. We therefore consider only the role of diffusion and surface kinetics in our discussions.

The possible results of the interplay between diffusion and growth rate at the crystal-melt interface has been summarized in numerous studies (Burton et al., 1953; Albarede and Bottinga, 1974; Kröger, 1973; Dowty, 1976). When the rate of uptake of a major component is much faster than diffusion in the melt, the rate of growth is controlled by the rate of diffusion. When diffusion of the major component to the interface is fast relative to the rate of incorporation, the rate of growth is controlled by the interface attachment processes. In this case, trace-element incorporation is influenced by variables such as adsorption, ion exchange, growth mechanisms, surface configuration, interface roughness, and temperature (T, ΔT). Can we differentiate between the importance of diffusion and interface kinetics in sector enrichments? If we choose the latter as the most important, can we identify the dominant variables?

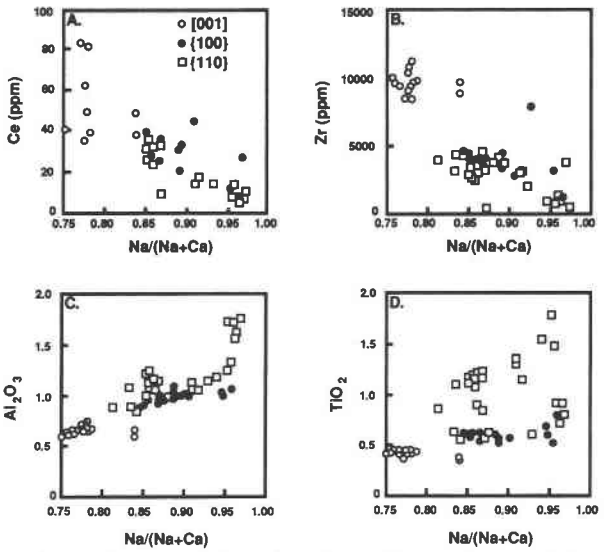

Fig. 3. Sector variability in major and trace elements. (**A**) Ce vs. Na/(Na + Ca). (**B**) Zr vs. Na/(Na + Ca). (**C**) Al_2O_3 vs. Na/(Na + Ca). (**D**) TiO_2 vs. Na/(Na + Ca).

Development of sector zoning in pyroxenes is a metastable phenomenon (Dowty, 1976; Shimizu, 1981). Yet that does not necessarily imply whether interface kinetics or diffusion is the dominant process in sector formation or relative sector trace-element enrichments. Generally, in large magma bodies such as represented by the Ilímaussaq alkaline intrusion, crystallization proceeds at small undercoolings. Under these conditions, the rate-controlling growth process is the interface reactions (Kirkpatrick, 1974; Cahn, 1967). Where the ratio of growth rate to diffusion coefficient is high, such as in a rapidly cooled lava flow, diffusion is expected to be the important process. Sector-zoned pyroxenes occur in both thermal environments (Dowty, 1976). Sector-zoned aegirine, however, has only been documented in undersaturated, peralkaline plutonic rocks (Larsen, 1981) and in hydrothermal veins and vugs associated with peralkaline intrusions (Ranløv and Dymek, 1991).

Morphological differences may be attributed to the operative process. Short-range diffusion results in the development of a cellular morphology (Elbaum, 1959), which is reflected in the crystal form (spherulites, dendritic and skeletal crystals) and in patch-zoned regions that are rich in glass inclusions. Other features that may reflect short-range diffusion processes include mineral inclusions (i.e., apatite) that may reflect supersaturation at the boundary layer (e.g., Bacon, 1989) and irregular zoning, which may reflect the extension of surfaces beyond a boundary layer into a strongly supersaturated region (Anderson, 1984). The influence of surface kinetics on crystal growth is suggested by textural features such as tabular crystals with faceted morphology (Kirkpatrick, 1975), individual compositional zones that are thicker on curvy or irrational surfaces (Hartman, 1973; Kirkpatrick, 1975; Anderson, 1984), and the fact that the thickness of individual compositional zones varies on different growth surfaces (Dowty, 1976). A faceted morphology is evidence of a stable interface, whereas the nature of zoning thickness is dependent upon surface roughness, the rate of interface attachment, and surface morphology. The morphology of the aegirine indicates surface kinetics was a much more important growth process.

Experimental evidence (Lofgren et al., 1974) also indicates that sector zoning characteristics, as observed in the aegirine, form as a result of slower cooling rates (1.2 °C/h) compared with cellular textural features (430–2.5 °C/h). Plots of growth rate vs. undercooling (growth rate vs. ΔT, log growth rate vs. $1/T\Delta T$) for experimental sector-zoning studies by Kouchi et al. (1983) and surface microtopographic studies of these experimentally grown crystals indicate that surface kinetic reactions and surface nucleation mechanisms were important in sector growth (Kirkpatrick, 1975; Kouchi et al., 1983).

Observations concerning relative sector enrichments also shed light on the relative importance of diffusion vs. surface kinetics on trace-element behavior. The consistent lack of correlation between growth rate and incompatible element enrichment of sectors in clinopyroxene (compare augite and aegirine) also indicates that surface kinetics plays a more important role than diffusion in sector enrichments.

Surface kinetics

The interplay among the numerous variables involved in the reaction of the crystal-melt interface is probably important in dictating differences in enrichment among sectors of calcic clinopyroxene and between the same sectors in calcic clinopyroxene and aegirine. These variables include magma composition, temperature, the degree of supercooling, the attachment kinetics of SiO_3, adsorption

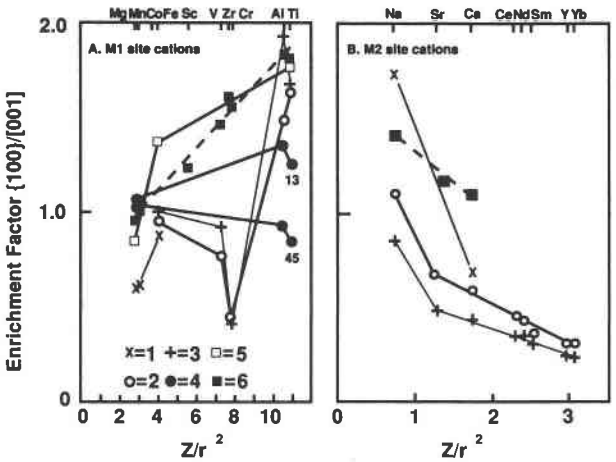

Fig. 4. Relative enrichment of elements in the {100} sector relative to the basal sector ({111} or [001]) as a function of the Coulomb interaction (ratio of the ionic charge of the element divided by the ionic radius squared). (**A**) M1 site cations. (**B**) M2 site cations. Index to data: 1 = Carpenter (1980), 2 and 3 = this study, 4 = Kouchi et al. (1983), 5 = Hollister and Gancarz (1971), and 6 = Shimizu (1981). The experimentally grown pyroxenes from Kouchi et al. (1983) are for supercooling of 13 and 45°.

and desorption kinetics of cations into surface sites, differences of surface atomic configurations, characteristics of individual sites (M1 vs. M2 sites, geometric flexibility), mechanisms of interface-controlled growth (continuous, surface nucleation, screw dislocation), and the nature of the ion exchange reactions occurring at the surface.

Shimizu (1981) concluded that in cases of rapid SiO_3^{-2} attachment, trace-element substitution into the M1 site in augite is based on both the configuration of the growth surfaces (the number of available M1 sites) and the ability of the cation to be retained in the structural site. The retention of a cation in a structural site is a function of the cation bond strength. The importance of the latter was based on the enrichment of the {100} prism sector relative to the $\{\bar{1}11\}$ basal sector in augite. If surface configuration were the only variable (four times as many M1 sites are available on the {100} growth surface as on the $\{\bar{1}11\}$ growth surface) the enrichment factor between the {100} sector and $\{\bar{1}11\}$ sector should consistently be equal to 4. However, Shimizu observed enrichment factors of 1–2 and a linear relationship between the enrichment factor and Coulomb interaction between cation and the M1 site (Z/r^2, where Z is ionic charge and r is ionic radius). This suggests that although the {100} growth surface had four times as many available M1 sites as did the basal $\{\bar{1}11\}$ growth surface, the {100} surface had a lower degree of trace-element adsorption or a higher degree of trace-element desorption (two to four times) than that of the $\{\bar{1}11\}$ surface.

Figure 4 shows the relationship between preferential enrichments of elements in the {100} prism sector relative to the basal sector and the strength of Coulomb interaction for cations that occupy the M1 site (Fig. 4A) and those that occupy the M2 sites (Fig. 4B). Data are from the aegirine of this study, augite (Shimizu, 1981; Hollister and Gancarz, 1971), sodic augite (Carpenter, 1980), and laboratory-grown calcic clinopyroxene (Kouchi et al., 1983). The study by Shimizu (1981) and this study are the only ones that report trace-element data.

The behavior of cations that occupy the M1 site generally shows an increase in the preferential enrichment of the prism sector relative to the basal sector with stronger Coulomb interaction. This is best illustrated with the data from Shimizu (1981). This behavior appears to confirm conclusions reached by Shimizu (1981) and Dowty (1976) that those cations that are most firmly bound to the site on the growth surface and therefore have a lower degree of desorption are those that have a high charge and a small ionic radius. Major- and minor-element data from Hollister and Gancarz (1971), Carpenter (1980), and Kouchi et al. (1983) show a similar relationship. However, unlike the data from Shimizu (1981), the data in the other studies show relationships that are not strictly linear, particularly those elements with the lowest Z/r^2 (Fig. 4). Comparisons of the {100} prism sector with the basal sector in the aegirine of this study shows even a further deviation from the observations made by Shimizu (1981) in augite. In particular, the {100} prism sector is depleted in Zr relative to the basal sector. These initial observations imply that coulombic interactions are not the only factor controlling sector enrichments.

If trace-element substitution were strictly a function of Coulomb interaction, a positive correlation similar to that observed by Shimizu for the M1 site cations (enrichment vs. Z/r^2) also would be observed for the M2 site cations. Observations from aegirine (this study) and augite indicate a preferential depletion in the {100} sector relative to the basal sector with increasing Coulomb interaction (Fig. 4B). The initial interpretation would be that those cations most firmly held in the M2 site are those with the least Coulomb interaction (Fig. 4B). This completely contradicts what we would expect and strongly suggests other surface kinetic processes are involved. These processes must account for (1) the lower degree of retention of particular trace elements in the {100} prism sector compared with the basal sector in aegirine, (2) the negative correlation between Coulomb interaction and relative sector enrichments of M2 site cations, and (3) the irregular enrichment behavior of Zr in the aegirine relative to augite.

Superimposed on factors such as the availability of sites and Coulomb interaction are the characteristics of a site that dictate its ability to accommodate a cation and differences in growth rate and growth mechanisms among sectors and surface reactions (i.e., coupled substitutions). Figure 5 illustrates the relationship among prism-basal sector enrichments, ionic radii, and cation valence. This diagram is similar to an Onuma diagram (McKay, 1989; Onuma et al., 1968) and reflects shifts in the optimum ionic radius a potential site can accommodate. In addition, the differences in cation site characteristics between

augite and aegirine appear to dictate the relative enrichments. The effect of the shift in the optimal radius is particularly noticeable in the M1 site. In aegirine, where the M1 site is dominated by Fe^{3+} (mean site radius = 62.5 pm) rather than Fe^{2+} (hedenbergite mean site radius = 73.1 pm), large M1 cations such as Zr are further offset from the optimum ionic radius for the M1 site. This accounts for the deviation of Zr in aegirine from linearity relative to augite, as observed by Shimizu (1981). It also suggests that the differences between hedenbergite and acmite in the ideal charge characteristic of the M1 site (Table 1) are less important. On the basis of only the ideal charge, the higher ideal charge of the M1 site in acmite (3.02) compared with hedenbergite (2.30) suggests Zr should be better accommodated in acmite.

The relative enrichments of all cations in the M2 site (Figs. 4 and 5) can be attributed to both optimal radius and ideal charge. Nearly identical M2 site radii for hedenbergite and acmite (Table 1) result in similar slopes in enrichment factors, whereas differences in optimal charge (hedenbergite = 1.79, acmite = 1.16) result in a higher enrichment factor for highly charged cations in augite. The negative correlation between Na/(Na + Ca) and many incompatible elements should not be interpreted as indicating that charge-balance reactions such as 2Ca (M2) ↔ Na (M2) + REE (M2) are not important. Rather, this correlation indicates the importance of the acmite substitution for the optimum radius of the M1 site and the ideal charge of the M2 site. In general, as a cation deviates from the optimal ionic radius and ideal charge of a site, it becomes increasingly incompatible.

In the pyroxenes from this study and other studies, the observation is that the sequence of relative sector enrichments does not strictly correlate to growth rate. The relative enrichments should be related to the number of relevant sites available on the growth surface and the mechanics of adsorption and desorption on that growth surface. As illustrated in this study, what is important to the latter is the actual nature of the sites, cation deviation from the optimal site size and ideal charge, and growth rate. The effect of this interrelationship on sector enrichment is illustrated in Figure 6.

In addition to relative growth rate, the growth mechanism should also be important in the incorporation of trace cations into a growth surface. In silicates such as pyroxene, lateral growth (surface-nucleation and screw dislocation mechanisms) rather than continuous growth appears to be the most common. Growth rate vs. supercooling relationships and the surface microtopography of laboratory-grown sector-zoned pyroxenes (Kouchi et al., 1983) suggest that both surface nucleation and screw dislocation mechanisms may be functioning. As illustrated by Hollister and Gancarz (1971), growth surface configuration may be dependent on growth mechanism. As the degree of supercooling will affect both crystal morphology and growth mechanism, the degree of supercooling may affect the configuration of the growth surface. This will have implications for the relative sector enrichments

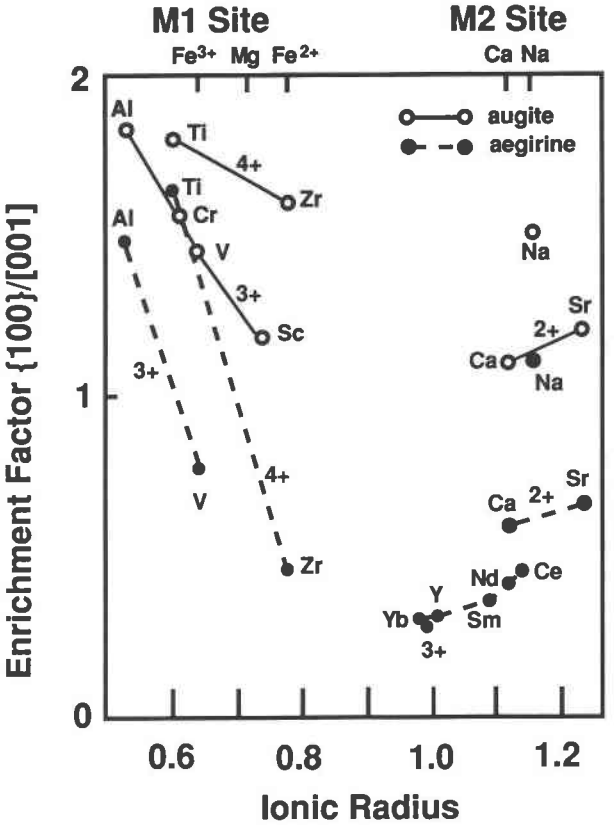

Fig. 5. Relative enrichment of elements in the {100} sector relative to the basal sector as a function of the ionic radius. Solid lines are augite data from Shimizu (1981). Dashed lines are aegirine data from this study.

(Kouchi et al., 1983). For example, in experiment with large degrees of supercooling (ΔT = 45°), clinopyroxene crystallized with the prism sector actually was depleted in Al and Ti relative to the basal sector. Other studies, by Reeder (1992) and Paquette and Reeder (1990a, 1990b), also illustrated the importance of growth mechanisms in trace-element behavior. Although supercooling may play an important role in producing relative sector enrichments in some cases, it is not likely to have been the controlling factor for the aegirine in this study because there is no evidence that a large degree of supercooling occurred in the Ilímaussaq magma.

In summary, the relative sector enrichments in pyroxene seem to correlate better with ionic radius (Fig. 5) than Z/r^2 (Fig. 4). Three observations, in particular, illustrate this point: (1) the depletion of Zr (M1 site, high Z/r^2) in the {100} sector relative to the [001] sector in aegirine, (2) the systematic enrichment of M2 site cations in {100} relative to [001] with decreasing Z/r^2 in both sodic and calcic pyroxenes, (3) the lower enrichment factor generally observable in aegirine vs. augite in most M2 site cations. These observations may be interpreted in two fundamentally different ways.

1. Crystal chemical or geometric factors dominate for

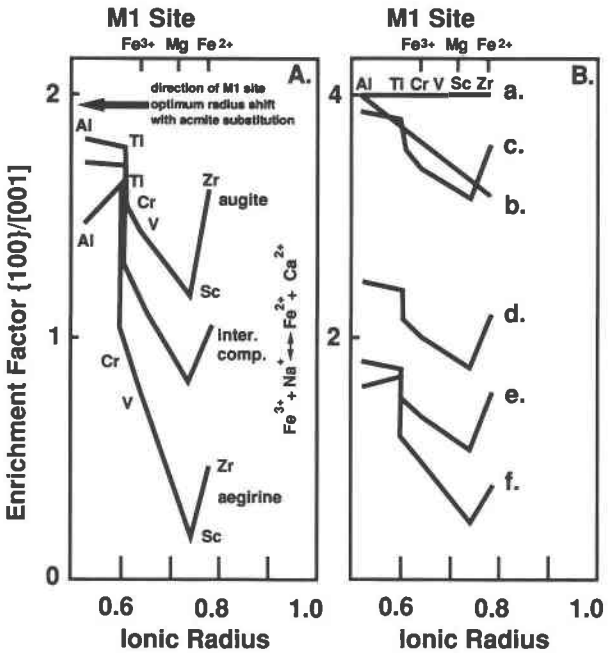

Fig. 6. Diagrammatic summary illustrating the influence of various factors on the relative enrichment of elements in the {100} sector relative to the basal sector of clinopyroxene as a function of ionic radius. (A) Influence of the acmite substitution ($Fe^{3+} + Na^{+} \leftrightarrow Fe^{2+} + Ca^{2+}$) on relative sector enrichments. (B) Illustration of the additive effect of a variety of factors on relative sector enrichments. (a) Pattern if only the number of M1 sites available on the growth surface were important. (b) Pattern if factor a and M1 site characteristics (optimum radius) were important. (c) Pattern if factors a, b, and Coulomb interaction (Z/r^2) were important. (d) In addition to factors a, b, and c, this pattern reflects differences between sectors in rate of growth, SiO_3^{-2} attachment, and cation adsorption and desorption. (e) Same as d but with a greater difference in growth rate between sectors. (f) Same as e but with a compositional shift influencing the M1 site characteristics (i.e., a shift of the optimum radius).

all elements in both aegirine and augite. In this interpretation, the hypothesis proposed by Nakamura (1973), Dowty (1976), and Shimizu (1981) is not valid, and the correlation between enrichment factors and Z/r^2 for M1 site cations evident in the data presented by Shimizu (1981) is fortuitous. In addition, the M2 site cations from this augite show the opposite relationship. In this case, site factors dominate for all elements in the aegirine. The acmite component ($NaFeSi_2O_6$) in each sector controls the abundance of the other elements through the influence of optimal radius for the M1 site and optimal charge for the M2 site. Although optimal radius for the M2 site dictates the slope of enrichment factors in Figure 5, the differences in the M2 site cation enrichments between augite and aegirine is mostly a function of the difference in ideal charge characteristics of the site. Each sector may have different partition coefficients because of different site size and ideal charge provided by different Na and Fe^{3+} contents. The difference in Na and Fe^{3+} content between sectors might be influenced by differences in elasticity of partially formed M1 and M2 sites in distinct crystallographic directions.

2. Site characteristics dominate for most minor and trace elements in aegirine because differences in structural components [Na/(Na + Ca) and $Fe^{3+}/(Fe^{2+} + Fe^{3+})$] among sectors make for large differences in site factors (optimal size and ideal charge). However, in contrast to 1, adsorption and desorption kinetics still controls Na/(Na + Ca) and $Fe^{3+}/(Fe^{2+} + Fe^{3+})$ sector enrichments in aegirine and thus is ultimately responsible for producing the trace-and minor-element sector zoning. Moreover, because augite has smaller differences in major structural components between sectors (compare characteristics of M1 and M2 sites between diopside and hedenbergite in Table 1), geometric factors might be less important in augite, and thus adsorption and desorption kinetics might be the dominant mechanism producing minor- and trace-element differences among sectors. In that case, the fact that a plot of sector enrichments in augite vs. ionic radius resembles an Onuma diagram is largely coincidence or is to be expected for any element lying along the Z/r^2 correlation line. It is, therefore, without genetic significance.

Acknowledgments

The authors wish to thank the Institute for the Study of Mineral Deposits, the Institute of Meteoritics, and the Geological Survey of Greenland for their support in this study. The analytical results on GGU material are published with the permission of the Geological Survey of Greenland. We also appreciate Nobu Shimizu's guidance during SIMS analysis at WHOI and his insight concerning the dynamics of surface kinetics on trace-element behavior. We also acknowledge the assistance of Mike Spilde in performing electron microprobe analyses on these samples. As always, J.J. Papike provided a reservoir of information concerning the crystal chemistry of pyroxene and unlimited enthusiasm. Hugh E. O'Brien and Gordon McKay provided insightful reviews that improved the overall quality of the manuscript. This research was supported by NSF grant RII-89-02066 (to C.K.S.).

References cited

Albarede, F., and Bottinga, Y. (1972) Kinetic disequilibrium in trace element partitioning between phenocrysts and host lava. Geochimica et Cosmochimica Acta, 26, 141–156.

Anderson, A.T. (1984) Probable relations between plagioclase zoning and magma dynamics, Fuego Volcano, Guatemala. American Mineralogist, 69, 660–676.

Bacon, C.R. (1989) Crystallization of accessory phases in magmas by local saturation adjacent to phenocrysts. Geochimica et Cosmochimica Acta, 53, 1055–1066.

Bence, A.E., and Albee, A.L. (1968) Empirical correction factors for the electron microanalysis of silicates and oxides. Journal of Geology, 76, 382–403.

Bence, A.E., and Papike, J.J. (1971) A martini-glass clinopyroxene from the Moon. Earth and Planetary Science Letters, 10, 245–251.

——— (1972) Pyroxenes as recorders of lunar basalt petrogenesis: Chemical trends due to crystal-liquid interactions. Proceedings of Lunar and Planetary Science, 3, 431–469.

Bence, A.E., Cameron, K., and Papike, J.J. (1970) Sector zoning in calcic clinopyroxenes (abs.). Eos, 51, 435.

Burton, J.A., Prim, R.C., and Slichter, W.P. (1953) The distribution of solute in crystals grown from the melt. Journal of Chemistry and Physics, 21, 1987–1996.

Cahn, J.W. (1967) On the morphological stability of growing crystals. In H.S. Peiser, Ed., Crystal growth, 856 p. Pergamon, Oxford, England.

Cameron, M., and Papike, J.J. (1981) Structural and chemical variations in pyroxene. American Mineralogist, 66, 1–50.

Cameron, M., Sueno, S., Prewitt, C.T., and Papike, J.J. (1973) High-temperature crystal chemistry of acmite, diopside, hedenbergite, jadeite, spodumene, and ureyite. American Mineralogist, 58, 594–619.

Caporuscio, F.A., and Smyth, J.R. (1990) Trace element crystal chemistry of mantle eclogites. Contributions to Mineralogy and Petrology, 105, 550–561.

Carpenter, M.A. (1980) Composition and cation order variations in a sector-zoned blueschist pyroxene. American Mineralogist, 65, 313–320.

Clark, J.R., Appleman, D.E., and Papike, J.J. (1969) Crystal-chemical characterization of clinopyroxene based on eight new structure refinements. Mineralogical Society of America Special Paper, 2, 31–50.

Czamanske, G.K., and Atkin, S.A. (1985) Metasomatism, titanian acmite, and alkali amphiboles in lithic-wacke inclusions within the Coyote Peak diatreme, Humboldt County, California. American Mineralogist, 70, 499–516.

Deer, W.A., Howie, R.A., and Zussman, J. (1978) Rock-forming minerals, vol. 2A, Single-chain silicates, 668 p. Wiley, New York.

Downes, M.J. (1974) Sector and oscillatory zoning in calcic augites from Mt. Etna, Sicily. Contributions to Mineralogy and Petrology, 47, 187–196.

Dowty, E. (1976) Crystal structure and crystal growth. II. Sector zoning in minerals. American Mineralogist, 61, 460–469.

——— (1977) The importance of adsorption in igneous partitioning of trace elements. Geochimica et Cosmochimica Acta, 41, 1643–1646.

Elbaum, C. (1959) Substructures in crystals grown from the melt. In B. Chalmers, and R. King, Eds., Progress in metal physics, vol. 8, 438 p. Pergamon, London.

Ferguson, A.K. (1973) On hour-glass sector zoning in clinopyroxene. Mineral Magazine, 38, 321–325.

Ferguson, J. (1964) Geology of the Ilímaussaq alkaline intrusion, South Greenland. Description of map and structure. Meddr Grøland, 172, 1–82.

——— (1970) The significance of the kakortokite in the evolution of the Ilímaussaq Intrusion, South Greenland. Meddr Grøland, 186, 193.

Harkins, E., and Hollister, L.S. (1977) Sector zoning of clinopyroxene from a weakly metamorphosed diabase. American Mineralogist, 62, 390–394.

Hartman, P. (1973) Structure and morphology. In P. Hartman, Ed., Crystal growth: An introduction, p. 367–402. North-Holland, Amsterdam.

Hollister, L.S. (1970) Origin, mechanism, and consequences of compositional sector-zoning in staurolite. American Mineralogist, 55, 742–766.

Hollister, L.S., and Gancarz, A.J. (1971) Compositional sector-zoning in clinopyroxene from the Narce area, Italy. American Mineralogist, 56, 959–979.

Irving, A.J., and Frey, F.A. (1984) Trace element abundances in megacrysts and their host basalts: Constraints on partition coefficients and megacryst genesis. Geochimica et Cosmochimica Acta, 48, 1201–1221.

Kirkpatrick, R.J. (1974) The kinetics of crystal growth in the system $CaMgSi_2O_6$-$CaAl_2SiO_6$. American Journal of Science, 273, 215–242.

——— (1975) Crystal growth from the melt: A review. American Mineralogist, 60, 798–814.

——— (1981) Kinetics of crystallization of igneous rocks. In Mineralogical Society of America Reviews in Mineralogy, 8, 398 p.

Kouchi, A., Suqawara, Y., Kashima, K., and Sunaqawa, I. (1983) Laboratory growth of sector zoned clinopyroxenes in the system $CaMgSi_2O_6$-$CaTiAl_2O_6$. Contributions to Mineralogy and Petrology, 83, 177–184.

Kröger, F.A. (1973) The chemistry of imperfect crystals (2nd edition), vol. 1, 313 p. North-Holland, Amsterdam.

Larsen, L.M. (1976) Clinopyroxene and coexisting mafic minerals from the alkaline Ilímaussaq intrusion, South Greenland. Journal of Petrology, 17, 258–290.

——— (1977) Aenigmatites from the Ilímaussaq intrusion, South Greenland: Chemistry and petrological implications. Lithos, 10, 257–270.

——— (1979) Distribution of REE and other trace elements between phenocrysts and peralkaline undersaturated magmas, exemplified by rocks from the Gardar igneous province, South Greenland. Lithos, 12, 303–315.

——— (1981) Sector zoned aegirine from the Ilímaussaq alkaline intrusion, South Greenland. Contributions to Mineralogy and Petrology, 76, 285–291.

Lasaga, A.C. (1981) Implications of a concentration-dependent growth rate on the boundary layer crystal-melt model. Earth and Planetary Science Letters, 56, 429–434.

Leung, J.S. (1974) Sector-zoned titanaugites: Morphology, crystal chemistry, and growth. American Mineralogist, 59, 127–138.

Lofgren, G.E., Donaldson, C.H., Williams, R.J., Mullins, O., and Usselman, T.M. (1974) Experimentally reproduced textures and mineral chemistry of Apollo 15 quartz normative basalts. Proceedings of the 5th Lunar Science Conference, 549–567.

Loomis, T.P. (1981) An investigation of disequilibrium growth processes of plagioclase in the system anorthite-albite-water by methods of numerical simulation. Contributions to Mineralogy and Petrology, 81, 219–229.

Mahood, G.A., and Stimac, J.A. (1990) Trace-element partitioning in pantellerites and trachytes. Geochimica et Cosmochimica Acta, 54, 2257–2276.

McKay, G. (1989) Partitioning of rare earth elements between major silicate minerals and basaltic melts. In Mineralogical Society of America Reviews in Mineralogy, 21, 45–77.

Nakamura, Y. (1973) Origin of sector-zoning of igneous clinopyroxenes. American Mineralogist, 58, 986–990.

Nakamura, Y., and Coombs, D.S. (1973) Clinopyroxenes in the Tawhiroko tholeiitic dolerite at Moeraki, northeastern Otago, New Zealand. Contributions to Mineralogy and Petrology, 42, 213–228.

Nielsen, T.F.D. (1979) The occurrence and formation of Ti aegirines in peralkaline syenites. Contributions to Mineralogy and Petrology, 69, 236–244.

Onuma, N., Higuchi, H., Wakita, H., and Nagasawa, H. (1968) Trace element partition between two pyroxenes and the host lava. Earth and Planetary Science Letters, 5, 47–51.

Paquette, J., and Reeder, R.J. (1990a) New types of compositional zoning in calcite: Insights into crystal-growth mechanisms. Geology, 18, 1244–1247.

——— (1990b) Surface symmetry constraints on compositional zoning and cation ordering during crystal growth. Geological Society of America Abstracts with Programs, 22, A216.

Ranløv, J., and Dymek, R.F. (1991) Compositional zoning in hydrothermal aegirine from fenites in the Proterozoic Gardar Province, South Greenland. European Journal of Mineralogy, 3, 837–853.

Reeder, R. (1992) Intrasectoral zoning in dolomite: Further evidence for surface structural control on element incorporation during crystal growth. V.M. Goldschmidt Conference Program and Abstracts, A88.

Robinson, P. (1980) The composition space of terrestrial pyroxenes-internal and external limits. In Mineralogical Society of America Reviews in Mineralogy, 7, 419–494.

Shaw, H.R. (1974) Diffusion of H_2O in granitic liquids: Part 1, Experimental data; Part II, Mass transfer in magma chambers. In A.W. Hofmann, B.J. Giletti, H.S. Yoder, Jr., and R.A. Yund, Eds., Geochemical transport and kinetics. Carnegie Institution of Washington, Publication 634, 353 p.

Shearer, C.K., Papike, J.J., Simon, S.B., Galbreath, K.G., and Shimizu, N. (1989) An ion microprobe study of the intra-crystalline behavior of REE and selected trace elements in pyroxene from mare basalts with different cooling and crystallization histories. Geochimica et Cosmochimica Acta, 53, 1041–1054.

Shearer, C.K., Papike, J.J., and Spilde, M.N. (1991) Pyroxene/melt trace element behavior: A study of pyroxenes from the Valley of Ten Thousand Smokes, Alaska. Geophysical Research Letters, 18, 1557–1560.

Shimizu, N. (1981) Trace element incorporation into growing augite phenocryst. Nature, 289, 575–577.

Shimizu, N., and Hart, S.R. (1981) Isotope fractionation in secondary ion mass spectrometry. Journal of Applied Physiology, 53, 1301–1311.

Smyth, J.R. (1992) Crystal structure controls on element partitioning in geologic systems. V.M. Goldschmidt Conference Program and Abstracts, A-105.

Smyth, J.R., and Bish, D.L. (1988) Crystal structures and cation sites in the rock-forming minerals, 386 p. Allen Unwin, London.

Strong, D.F. (1969) Formation of the hour-glass structure in augite. Mineralogy, 37, 472–479.

Thompson, R.N. (1972) Oscillatory and sector zoning in augite from a Vesuvian lava. Carnegie Institution of Washington Year Book, 71, 463–470.

Ussing, N.V. (1912) Geology of the country around Julianehaab, Greenland. Meddr Grønland, 38, 376 p.

Manuscript received October 21, 1992
Manuscript accepted November 15, 1993

ERRATUM

Plagioclase-melt equilibria in hydrous systems, by T. B. Housh and J. F. Luhr (v. 76, p. 477–492). Some of the plagioclase compositions shown in Figure 2 were incorrectly plotted. A corrected version of the figure is given below.

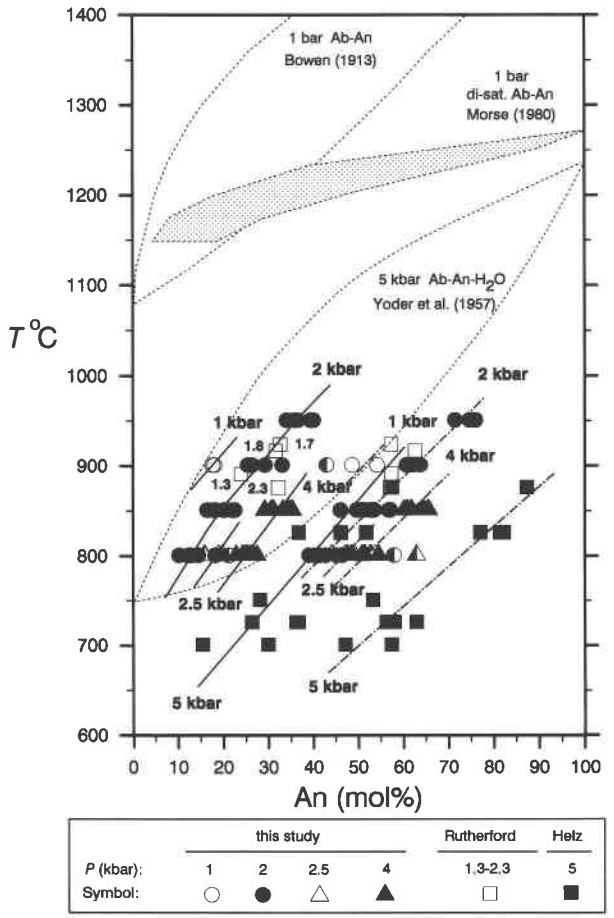

Fig. 2. Albite-anorthite binary diagram showing the 1-bar liquidus-solidus loop of Bowen (1913) and the 5-kbar H_2O-saturated loop of Yoder et al. (1957). Also shown is the collapse of the loop when projected from diopside saturation in the system diopside-albite-anorthite (Wyllie, 1963; Morse, 1980). Symbols show plagioclase and projected glass compositions from this study, Helz (1976), and Rutherford et al. (1985). Multicomponent glass compositions are plotted as 100[normative an/(an + ab)]. Half-solid symbols indicate the eight samples whose plagioclase or glass compositions deviate from the general trends and are deleted from the modeling. Values near open squares indicate experimental pressures in kilobars for data from Rutherford et al. (1985). Solid and dash-dotted lines labeled 1, 2, 2.5, 4, and 5 kbar indicate mean loci of projected isobaric melt and plagioclase compositions, respectively.